Supporting Information

Comparative Investigation of the Deactivation Behaviors over HZSM-5 and HSAPO-34 Catalysts during Low-temperature Methanol Conversion

Liang Qi[ab], Jinzhe Li[a], Linying Wang[a], Chan Wang[a], Lei Xu[a] and Zhongmin Liu*[a]*

[a] National Engineering Laboratory for Methanol to Olefins, Dalian National Laboratory for Clean Energy, iChEM (Collaborative Innovation Center of Chemistry for Energy Materials), Dalian Institute of Chemical Physics, Chinese Academy of Sciences, Dalian 116023, People's Republic of China;

[b] University of Chinese Academy of Sciences, Beijing 100049, P. R. China;

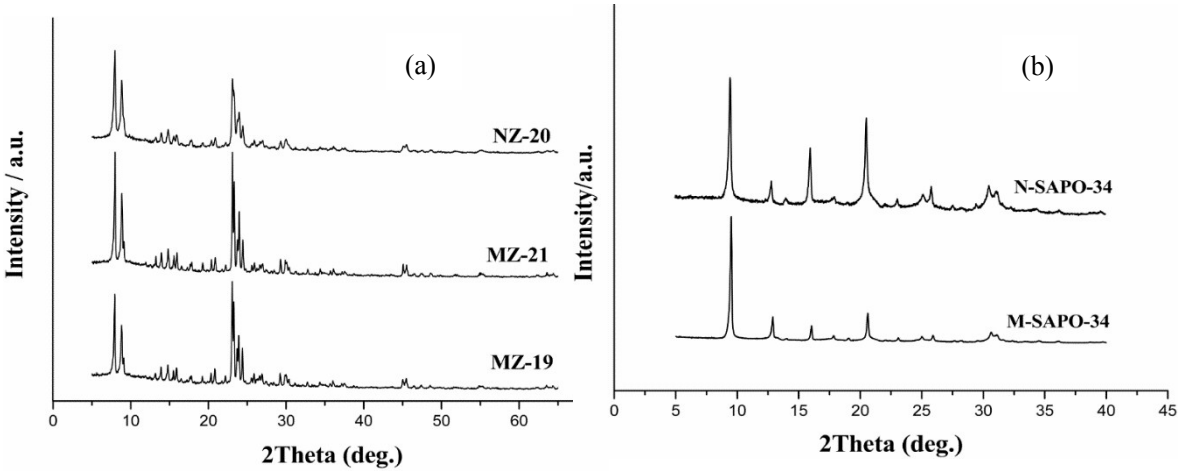

Figure S1. XRD patterns of HZSM-5 (a) and HSAPO-34 (b) catalysts

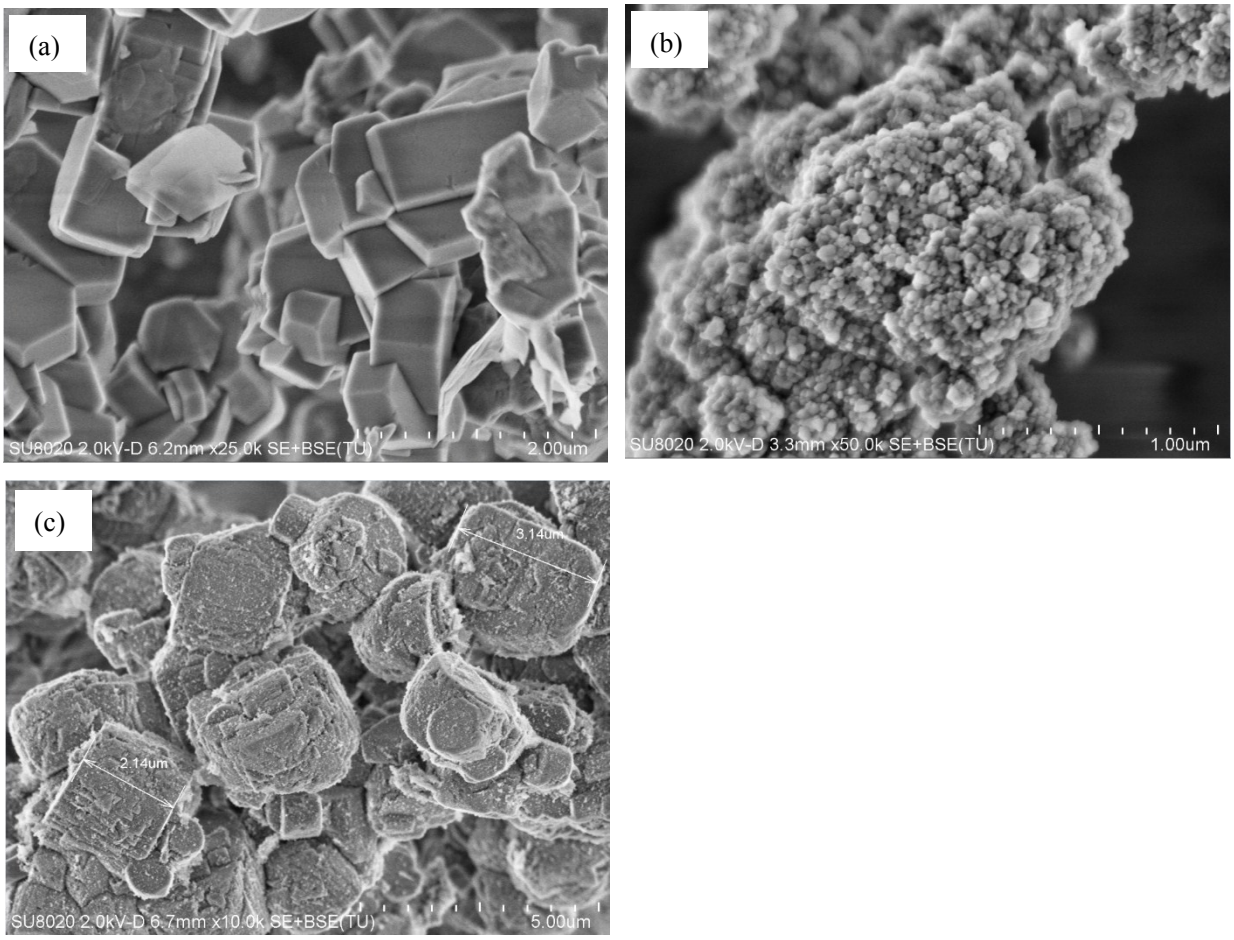

Figure S2. SEM images of the tested samples for MZ-19 (a), NZ-20 (b) and MZ-21 (c).

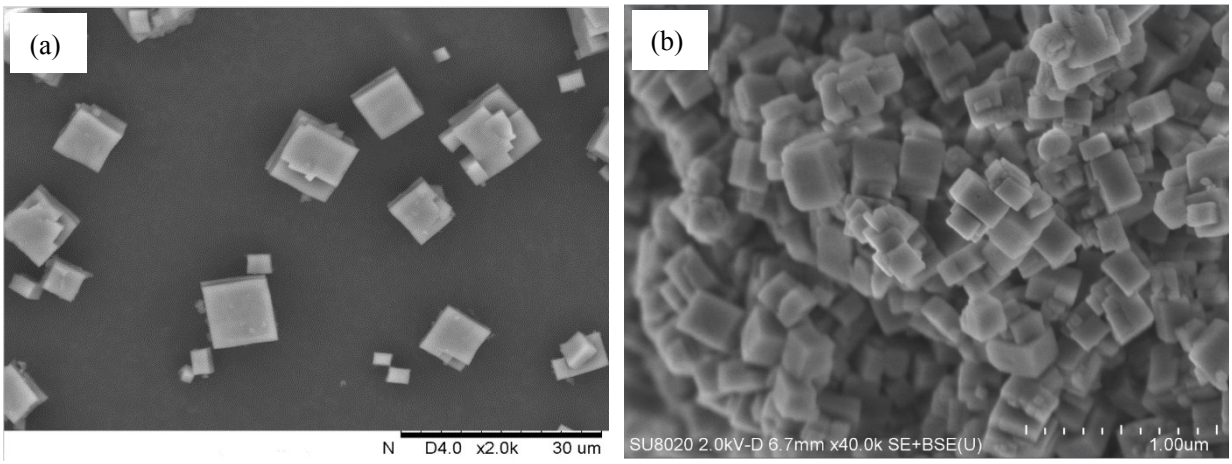

Figure S3. SEM images of the tested samples for M-SAPO-34 (a) and N-SAPO-34 (b).

Table S1 Elemental composition and N_2 sorption results for HZSM-5 samples

Sample	Si/Al[a]	$S_{micro}(m^2/g)$[b]	$S_{ext}(m^2/g)$[b]	$V_{micro}(mL/g)$
MZ-19	19	318	22	0.147
MZ-21	21	336	20	0.154
NZ-20	20	243	161	0.12

[a] XRF.

[b] t-Method.

Table S2. Elemental composition and N_2 sorption results for HSAPO-34 samples

Sample	Si/(Si+Al+P) (%)[a]	S_{micro} (m^2/g)[b]	S_{ext} (m^2/g)[b]	$V_{micro}(mL/g)$
M-SAPO-34	8.7	399	5	0.195
N-SAPO-34	8.8	479.3	50.3	0.22

[a] XRF

[b] t-method

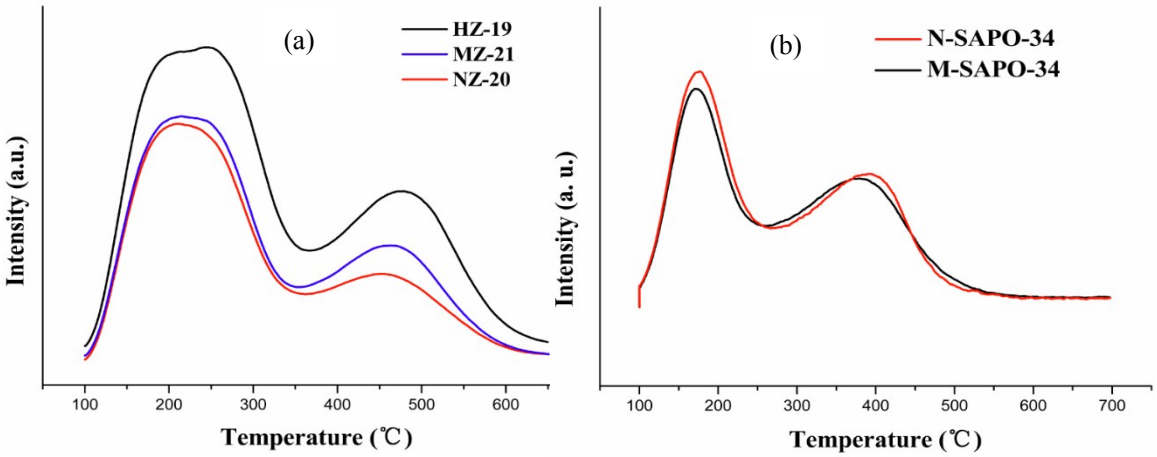

Figure S4. NH_3-TPD profiles of the HZSM-5 (a) and HSAPO-34 catalysts (b).

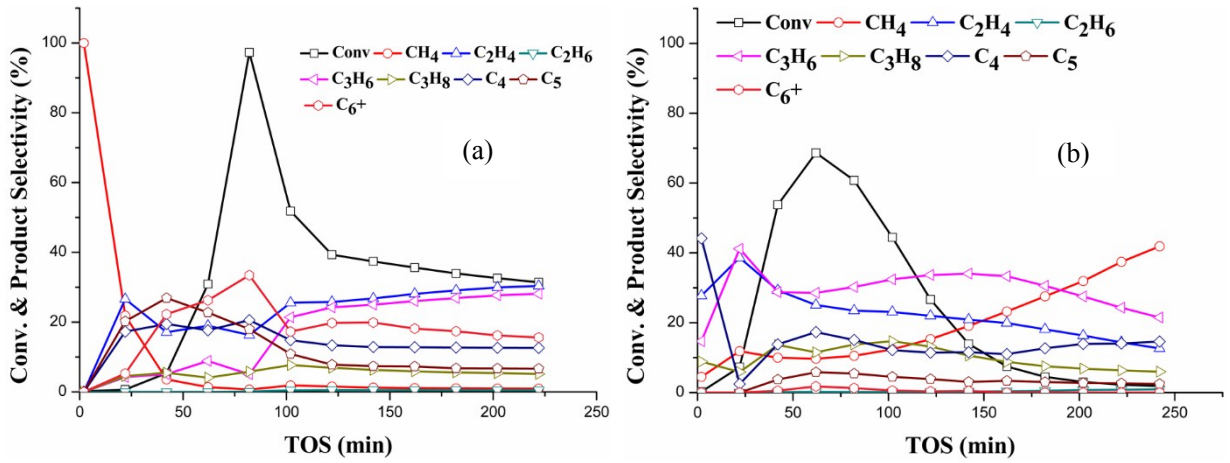

Figure S5. Change of methanol conversion and product distribution with TOS at 270 ^{o}C for MZ-19 (a) and M-SAPO-34 (b) catalyst.

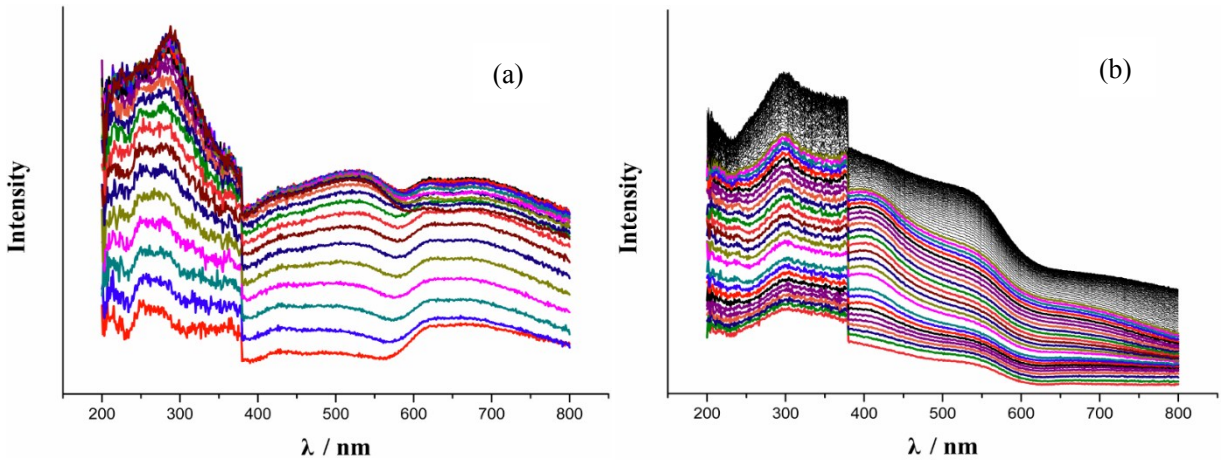

Figure S6. In situ UV/vis spectra recorded during the MTH reaction at 270 ^{o}C over MZ-19 (a) and M-SAPO-34 (b).

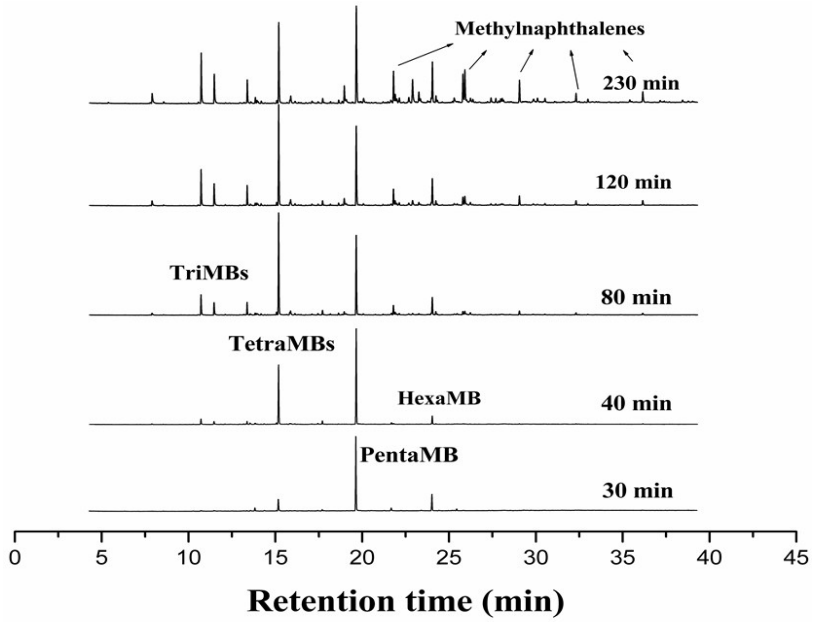

Figure S7. GC-MS analysis of retained materials retained species after methanol conversion at 280 ^{o}C for MZ-19.

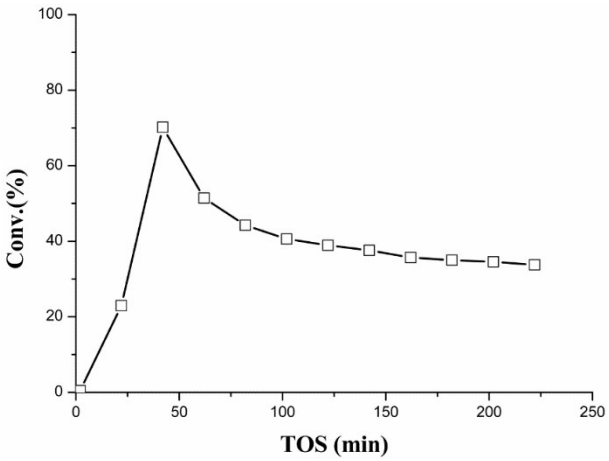

Figure S8. Methanol conversion as a function of TOS at 270 ^{o}C over MZ-21 catalyst.